Supplement of Atmos. Chem. Phys., 20, 1089–1103, 2020
https://doi.org/10.5194/acp-20-1089-2020-supplement

Atmospheric Chemistry and Physics
Open Access
EGU

Supplement of

No anomalous supersaturation in ultracold cirrus laboratory experiments

Benjamin W. Clouser et al.

Correspondence to: Benjamin W. Clouser (bclouser@uchicago.edu) and Elisabeth J. Moyer (moyer@uchicago.edu)

S1 Instrument Comparison

In the IsoCloud campaign, three water instruments provided data used in this analysis. ChiWIS and SP-APicT both provided water vapor measurements, and APeT provided measurements of total water (vapor + ice). SP-APicT and APeT are both spectrometers and use the same spectral line to make their measurements. However, SP-APicT is a single pass *in situ* instrument and APeT is an extractive instrument that uses a Herriot cell for increased path length. ChiWIS is a multi-pass, *in situ* instrument that uses a different spectral line to make its water vapor measurement. Before these instruments can be used in the data analysis, some differences between them must be reconciled.

S1.1 Low Temperature Performance

Water measurements are notoriously difficult to make at low temperatures due to the 'stickiness' of the water molecule and the large range of H_2O concentrations (roughly four orders of magnitude) in the atmosphere. In the IsoCloud 4 campaign the ice-wall experiments provide a way to gauge the low temperature performance of the instruments. In such experiments water is added to the chamber until a large enough coating of ice is formed on the wall to hold the saturation at 80-90% of the MK value calculated from the chamber gas temperature. Figure S1 shows the fractional deviation of ChiWIS (black) and SP-APicT (blue) against the saturation vapor pressure of the chamber gas. At temperatures above 205 K SP-APicT and ChiWIS show a nearly constant deviation, but at temperatures below 205 K, SP-APicT becomes almost 10% higher. This pattern indicates contamination at low water or perhaps the presence of data retrieval errors for a small spectral line.

The behavior of the APeT instrument is very similar to that of SP-APicT at temperatures above 205 K, but it shows larger deviations at low temperatures. At the lowest temperatures, ice lingers in the chamber for a very long time, and there is even residual ice present at the start of the subsequent experiment. (The experiments for which this is the case also lack Welas 1 data and they are not included in the analysis.) However, even in experiments for which this is not the case, APeT shows a larger increase than SP-APicT at low temperatures, which may be due to ice forming on the instrument's inlet.

S1.2 Linestrength Errors

Spectrometers are subject to linestrength errors which typically manifest as multiplicative offsets between instruments. To quantify the magnitude of this error between the instruments used here, we look at their pre-experiment values when there is no ice in the chamber. Figure S2 shows the percent deviation between ChiWIS and SP-APicT during the 60 seconds before pumping begins for all experiments in the IsoCloud 4 campaign. For temperatures above about 205 K, this deviation is quite linear, and on average SP-APicT is 1.5% below ChiWIS. Below 205 K, the deviation increases strongly, probably due to contamination within the SP-APicT instrument.

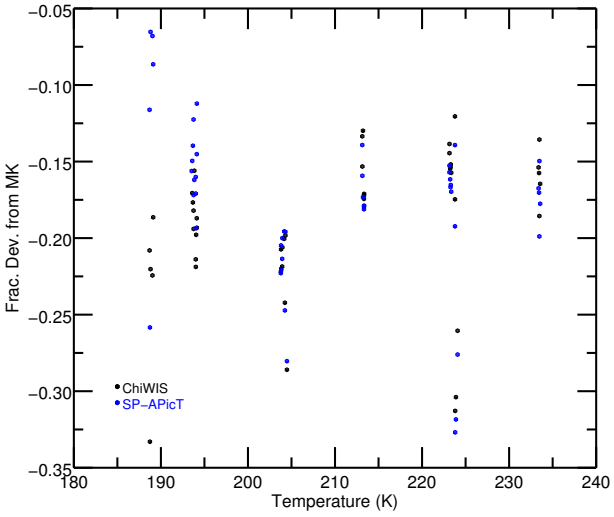

Figure S1. Fractional deviation of ChiWIS and SP-APicT against MK saturation. The deviations and temperatures are the average values of the 60 second period before the pump turns on. The 45 experiments for which there is suitable data to calculate this average are plotted here. ChiWIS points are in black, and SP-APicT points are in blue.

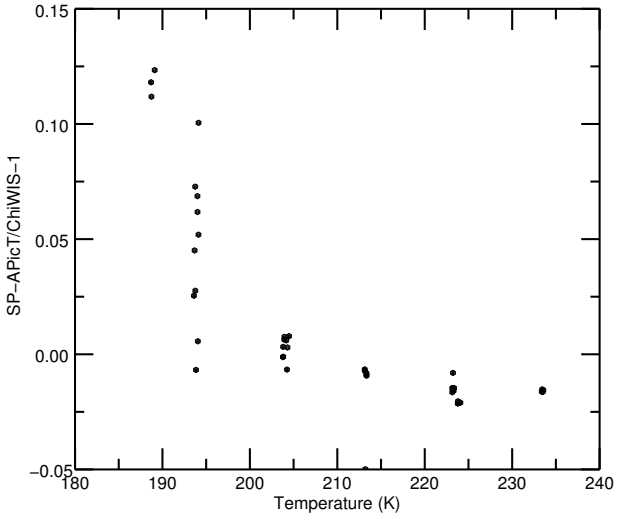

Figure S2. Fractional deviation between SP-APicT and ChiWIS plotted vs temperature. The average deviations and temperatures are calculated in the 60 seconds before the pump turns on.

S1.3 Absolute Errors

Due to its relative lack of contamination and higher precision at low temperatures, ChiWIS is used to calculate chamber

ice content and growth rate. To make this calculation, APeT is first scaled up by 1.5%. However, there is typically still a small, apparently random difference between the instruments at temperatures above 205 K, and a larger difference at lower temperatures due to APeT reporting higher values in that range. These remaining differences are taken to be constant, absolute offsets, and are subtracted from the whole experiment.

S2 Experiments

IsoCloud experiments are strongly influenced not only by the properties of the ice cloud (number concentration, temperature, etc.), but also by the preparation and behavior of the wall. This section lays out the different ways in which wall flux can affect an experiment and quantifies these effects.

S2.1 Types of Experiments

Figure S3 shows the change in S that occurs after turning the pumps off. The change is calculated as the average S of the 200 seconds before the pump turns off minus the average S of the 200 seconds after it turns off. This difference reveals several different categories of experiment. Those with negative ΔS are typically ones that show a 'bump' in S after the pumps turn off and the chamber rapidly warms. This bump may indicate that the ice cloud is not decaying uniformly across the chamber. Since heat flux enters the chamber through the walls, it follows that cirrus near the walls would be the first to sublimate, although the mixing fan will mitigate this behavior. However, the net effect of this inhomogeneous sublimation across the chamber will be to report a concentration (which is, roughly speaking, an average across the laser's path) which is higher than the expected saturation value calculated from the chamber's thermocouples, which are close to the centerline of the chamber. Experiments 8, 11, 17, and 21 are good examples of this type of experiment, which occurs at all temperature ranges. However, the magnitude of the effect is quite small and it only occurs when the cloud is rapidly warming and sublimating, so its overall effect on retrieved saturation vapor pressures is small.

Some experiments like the ~230 K day and 46-48 show a large positive ΔS because the cloud has already partially decayed in the latter time interval. These are experiments in which the wall's influence on the ice cloud is relatively unimportant, which may be due to relatively low wall flux (cf. Figure S4), which implies that relatively little ice mass is added to the cloud beyond that which is available in the vapor.

The large positive ΔS in the colder experiments is the wall-dominated pattern that is most apparent in experiments 30, 31, and 35. In these experiments the flux from the wall is quite large compared to the uptake capacity of the ice cloud, and a significant supersaturation is necessary to drive enough growth to balance the wall flux. In all ice-wall experiments included in the analysis the ice flux roughly balances the ice growth by the end of pumping, as evidenced by the measured saturation settling to a nearly constant value.

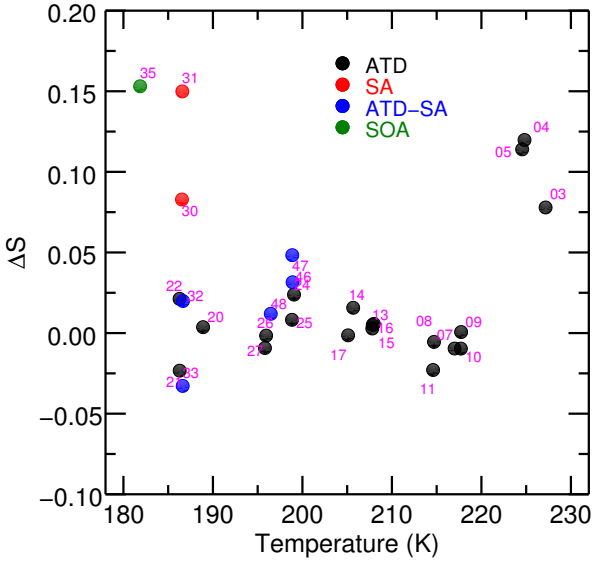

Figure S3. Difference between pre- and post-pump-turnoff values plotted against pre-turnoff average temperature. The difference is calculated by averaging the saturation values for 200 seconds before the pump turns off and 200 seconds after the pump turns off, then subtracting the post-turnoff value from the pre-turnoff value. Experiments are labeled by number and colored by aerosol/IN type.

S2.2 Wall Flux

In experiments with ice covered walls, the wall flux drives cirrus growth as long as the vapor pressure of the chamber gas is less than the saturation vapor pressure set by the wall ice. This is typically the case whenever there is a reasonably thick, established ice cloud in the chamber and its temperature is lower than that of the walls.

Figure S4 shows the maximum cirrus depositional flux and typical wall flux for each experiment included in the analysis. The maximum depositional flux occurs shortly after the cloud nucleates and is taken to be a measure of the uptake capacity of the chamber cirrus in a given experiment. Peak deposition scales very nearly with the saturation vapor pressure over ice. The typical wall flux value is calculated as the average wall flux during the last 200 seconds of pumping. By this time in most experiments, the gas temperature has settled to a nearly constant value, which means that the difference in saturation vapor pressure over cirrus ice and saturation vapor pressure over wall ice in nearly constant as well, since the wall temperature is almost constant through experiments. This constant difference in vapor pressures is the cause of the nearly constant wall flux in this time interval.

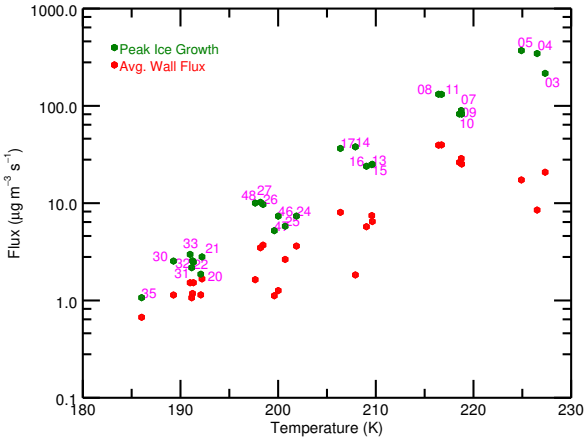

Figure S4. Maximum depositional flux onto cirrus (green) and typical wall flux (red) for the 28 experiments included in the analysis. The maximum depositional flux occurs shortly after ice nucleation. The typical wall flux is the average of the wall flux during the 200 seconds prior to the pump turning off. The temperature of each point is the average temperature during the fit window. Experiments are labeled by their experiment number. Note that this analysis was conducted with fits which used the 2012 HITRAN parameters.

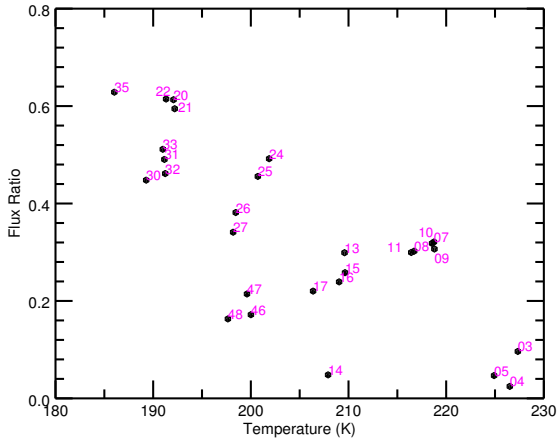

Figure S5. Ratio of typical wall flux to peak depositional flux onto cirrus plotted as a function of temperature. The temperature is the average temperature for each experiment's fit region, and each experiment is labeled by its experiment number. Wall flux tends to become less important as temperature increases. Note that this analysis was conducted with fits which used the 2012 HITRAN parameters.

Figure S5 shows the ratio of the average wall flux to the peak deposition for the 28 experiments included in the analysis. The wall flux becomes more important at lower temperatures because the typical wall flux does not drop off at low temperatures as quickly as cloud uptake does. There are no evident systematics in our results due to wall flux.

S2.3 Relaxation Times

Relaxation times back to pseudo-equilibrium are calculated for each measurement point using Equation (21) in Korolev and Mazin (2003):

$$\tau_p = \frac{1}{a_0 u_z + b_{i0} N_i \bar{r}_i} \tag{1}$$

Here N_i is the number of ice particles per cubic meter, $\bar{r}_i$ is the average ice particle radius, and u_z is the updraft speed, which we calculate from the rate of temperature change. The calculation of this time takes account cooling rate (effective updraft speed), ice particle number, and particle size to estimate the timescale for achieving a pseudo-equilibrium value. The remaining terms are defined as follows:

$$a_0 = \frac{g}{R_a T} \frac{L_i R_a}{c_p R_v T - 1} \tag{2}$$

$$a_3 = \frac{1}{q_v} + \frac{L_i^2}{c_p R_v T^2} \tag{3}$$

and

$$b_{i0} = a_3 \left(\frac{4\pi c \rho_i}{\rho_a} \left(\frac{\rho_i L_i^2}{k R_v T^2} + \frac{\rho_i R_v T}{e_i(T) D} \right) \right) \tag{4}$$

The remaining factors are defined as follows: g is the acceleration due to gravity, R_a is the specific gas constant of moist air, T is the vapor temperature, L_i is the specific heat of ice, c_p is the specific heat capacity of moist air at constant pressure, R_v is the specific gas constant of water vapor, q_v is the water vapor mass mixing ratio, c is the ice particle shape factor (taken to be 1 in this work), ρ_i is the density of ice, ρ_a is the density of air, e_i is the saturation vapor pressure over ice, and D is the diffusivity of water vapor in air. This approximation of the relaxation time is valid when the cloud's properties are not changing rapidly.

S3 Model Details

This section briefly talks about the calculation of instrumental uncertainties, then explores the sensitivity to assumptions about the accommodation coefficient and undercounting of particles by the Welas instrument. We find that the model is quite insensitive to assumptions about accommodation coefficient over a broad range, and that undercounting has little effect except at the coldest temperatures, where a small effect is possible.

S3.1 Instrumental uncertainty

For each experiment, we calculate a component of the uncertainty in retrieved vapor pressure that we term the 'instrumental uncertainty.' This quantity reflects the uncertainties associated with measurements of temperature, pressure, water vapor (ChiWIS and SP-APicT), total water (APeT), and ice particle number (Welas). The assumed distribution and stated magnitude of the uncertainties associated with each instrument are shown in Table S1.

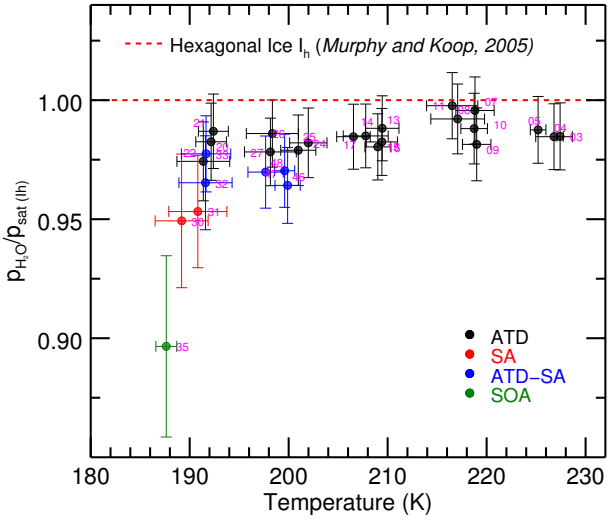

Figure S6. Model results showing only instrumental uncertainties, without linestrength errors, which are the same for all experiments. Results are scaled by Murphy-Koop (MK) saturation (red, dashed line) and plotted against average experiment temperature. Experiments are plotted with their experiment numbers in magenta.

The uncertainty on each retrieved parameter is generated by using the distributions and uncertainties of each measurement to generate a 2000 'new' data sets for each experiment, which are all then run through the model, resulting in a set of possible retrieved saturation vapor pressures for each point. The new data sets are generated by adding the appropriate noise into the original data sets at the correct magnitude to ensure the magnitude of uncertainty found in the new data is the same as that of the old data. The sets of retrieved saturation vapor pressures are nearly normally distributed, and the reported instrumental uncertainty is taken to be the standard deviation of a gaussian curve fit to the distribution. The distribution is generated from the set of vapor pressures by scaling them by MK saturation, then generating a histogram from the data set with a bin size of 0.1%.

Figure S6 shows the results of our analysis with only the instrumental uncertainty and temperature uncertainty plotted. Since the linestrength errors affect all experiments equally and in the same direction, plotting with only instrumental uncertainty better shows the relationships between individual experiments and groups of experiments.

Instrument	Uncertainty	Distribution
ChiWIS	$4 \cdot 10^{-4}$	Gaussian
SP-APicT	$5 \cdot 10^{-5}$	Gaussian
APeT	$5 \cdot 10^{-5}$	Gaussian
Pressure	1 hPa	Gaussian
Temperature	0.3° C	Gaussian
Welas 1 (conv.)	0.1	Gaussian
White Cell Len.	0.1%	Gaussian
ΔS due to ΔT	0.1%	Gaussian

Table S1. Uncertainties for each of the measured quantities used to model the vapor pressure in this work. Fractional uncertainties for the spectroscopic instruments are assumed to be minimum detectable absorptions, and are converted into uncertainties in mixing ratio using the HITRAN line parameters of the relevant spectral features, the pressure, and the temperature. The stated uncertainty in Welas 1 is a fractional uncertainty. All uncertainties are assumed to be normally distributed.

S3.2 Assumption of accommodation coefficient

The model is quite insensitive to assumptions about accommodation coefficient. The model outputs for experiments 16 and 30 are shown in Figure S7. The overall effect of decreasing the accommodation coefficient is to make the model more sensitive to temperature fluctuations in the data and to shift the model fits to slightly lower saturation vapor pressure. Assuming an accommodation coefficient of 0.2 instead of 1 results in an average decrease of 0.5% in the retrieved saturation vapor pressure. Wall dominated experiments such as 30 and 35 experience significantly larger decreases of about 1.5%. Physically, this decrease in retrieved saturation vapor pressure makes sense because if water vapor molecules attach to ice less efficiently, then a higher supersaturation is required to drive the observed growth. The only means by which the model can create a larger supersaturation is to decrease the assumed saturation vapor pressure.

Figure S8 shows the results of the saturation vapor pressure retrieval and uncertainty analysis when the model is run under the assumption that the accommodation coefficient is 0.2. Aside from the general decrease in the returned value, there is an overall increase in the width of the calculated error bars, which reflects the model's increased sensitivity to temperature fluctuations. However, this increase is quite small, and overall the model is quite insensitive to changes in accommodation coefficients and the assumption that $\alpha = 0.2$ does not change our interpretation of the results.

S3.3 Susceptibility to Ice Particle Number

The Welas 1 instrument has a lower diameter cutoff of $0.7\ \mu\mathrm{m}$, which introduces some potential complications for the analysis. During both nucleation and cloud decay there are a significant number of ice particles smaller than this which will not be counted. These regions are excluded by imposing an average radius cutoff of $0.85\ \mu\mathrm{m}$ on the fit range

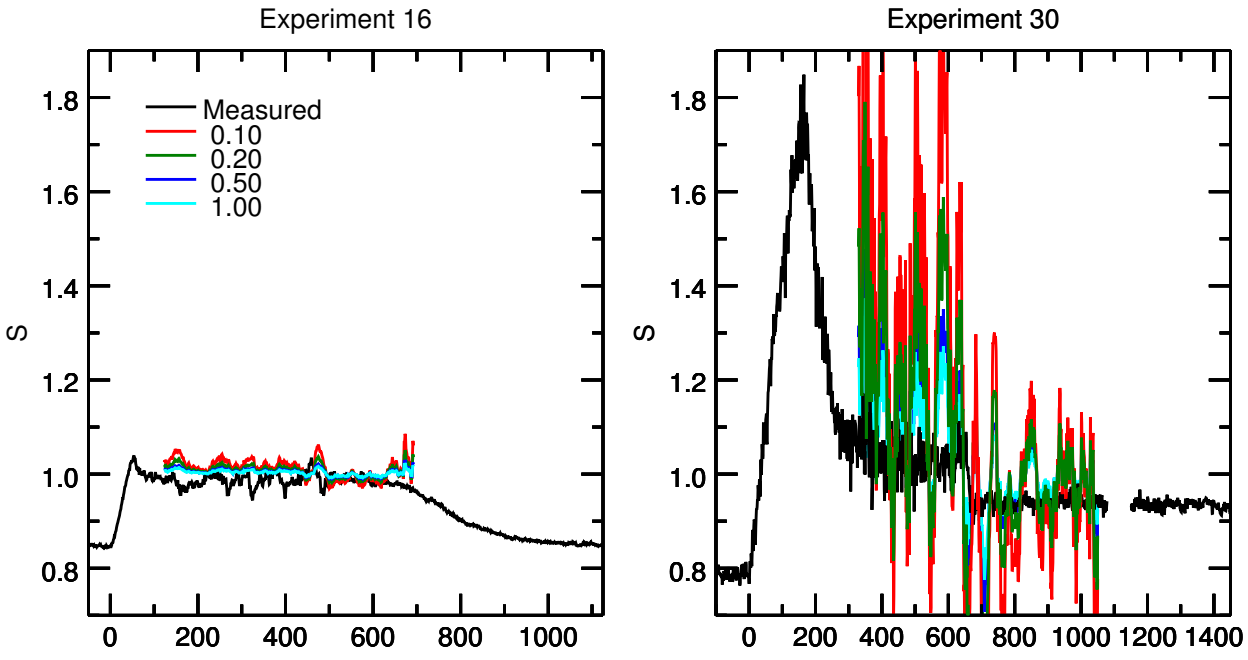

Figure S7. Model output for experiments 16 and 30 under different assumptions of accommodation coefficient. Observed and calculated saturations are plotted against the time from the start of the experiment in seconds. Measured data (black) is plotted on one-second intervals, and model output is smoothed by 30 points. Four different accommodation coefficient assumptions are shown in each figure: $\alpha = 0.10$ (red), $\alpha = 0.20$ (green), $\alpha = 0.50$ (blue), and $\alpha = 1.00$ (cyan). The data gap in experiment 30 at about 1100 seconds is due to a realignment of the chamber's White Cell mirrors.

of each experiment. However, this does not address persistent undercounting which may occur for experiments with low average particle size. Table S3 lists the maximum average particle radius for each experiment, and it is clear that at temperatures below 200 K particle size distributions may include a significant number of particles less than $0.7\ \mu\mathrm{m}$ in diameter. This undercounting will result in an overly large estimate of average particle size, and overestimates of per-particle growth rate as well, since fewer particles must account for the observed growth.

To get a very rough estimate of the magnitude of this effect we estimate particle size distributions for one of the low-temperature, small ice particle experiments. This estimate is made by fitting a log-normal distribution to the observed properties of the ice cloud. In the fit, the three lognormal parameters and saturation vapor pressure are free parameters, and they are used to estimate the number of ice particles observed by Welas 1, the number of ice particles observed by Welas 2 (which measures at a higher size range), the observed growth rate, and the mass of the ice cloud. These estimates are fit to the observed quantities, and yield physically reasonable values for the three lognormal parameters and the vapor pressure. These fits were performed on 30 second averages of experiments 9, 30, and 32 over the range where Welas 1 measures particle densities greater than $5\ \mathrm{cm}^{-3}$. The results of the fits to experiment 9 show the expected result that Welas 1 is counting almost all the particles present in the chamber due to their large size. The results of the fits to experiments 30 and 32 suggest that during the period of rapid ice growth just after nucleation the Welas 1 instrument may be measuring as little as 20% of the ice particles in the chamber, and during the established phase of the ice cloud about 50% of the particles are counted.

The latter number is relevant to the fit region, and to test for the presence of bias introduced by undercounting, we rerun the analysis under the assumption that there are 1.5, 2, and 5 times more particles in the chamber than Welas measured. Figure S9 shows the results for the 5x particles case. As stated in the main text, there is little movement in retrieved saturation vapor pressure values except at low temperatures, and the largest increase at low temperatures is about 2.0%. The experiments which show the most change in retrieved vapor pressure are those for which undercounting appears to be most likely. Experiments in which undercounting is not likely show very little change in retrieved vapor pressure; 23 of the 28 experiments show changes of less than 0.5%. These results indicated that even the largest possible undercountings due to small particle size do not change the results presented in this work.

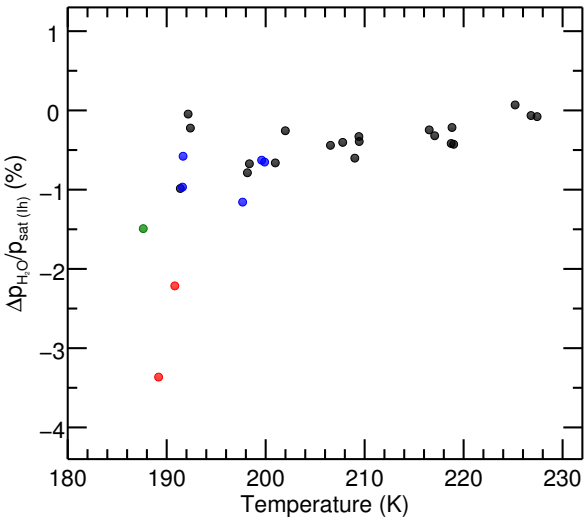

Figure S8. Percent difference in retrieved saturation vapor pressures between the case where the accommodation coefficient is assumed to be 0.2 and where it is assumed to be 1, which is the assumption made in the main text. Experiments are colored by aerosol/IN type and the temperature is the average value during the fit region. Assuming a lower accommodation coefficient drives the retrieved saturation vapor pressure lower for almost all experiments, since a larger supersaturation is then required to drive the observed growth. Experiments at the lowest temperatures are somewhat sensitive to assumptions about α, but for most experiments the shift is small. In any case, assuming that α is less than one results in lower retrieved vapor pressures overall, and does not affect the interpretation of results. Model uncertainties (not shown) are slightly higher when it is assumed that $\alpha = 0.2$, but again the difference is small.

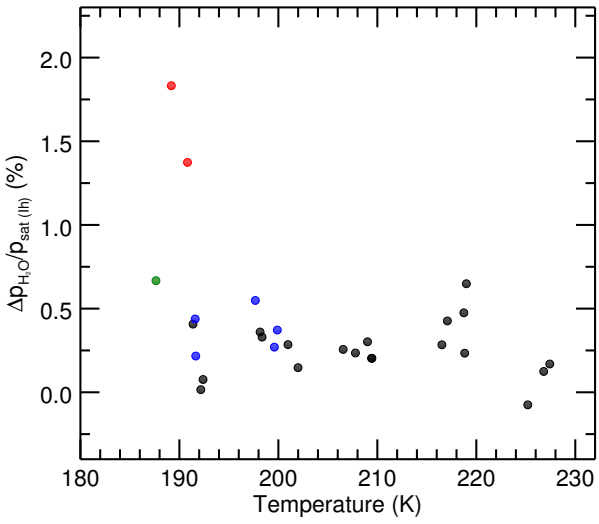

Figure S9. Percent difference in saturation vapor pressure retrievals between a model run which assumes 5x the number of observed ice particles, and the base case which assumes the observed concentrations presented in the main text. Experiments are colored by aerosol/IN type, and temperatures are the average temperature in the fit window. Assuming a higher concentration of ice particles in the chamber vapor pressure retrievals ~2% higher in some of the coldest experiments, which is consistent with the fact that these experiments have the smallest average radii and suffer from undercounting. These increases would tend to put the colder experiments somewhat more in line with the rest of the experiments, and do not change the interpretation of the results.

S4 HITRAN Version

The analysis in this manuscript was originally done using concentrations extracted from the raw spectra with parameters from the HITRAN 2012 database (Rothman et al., 2013). In the process of preparing this manuscript, the 2016 version of HITRAN was released (Gordon et al., 2017). This update contained important changes to the H_2O spectral feature used in this analysis, so the raw spectra were refit with the update parameters. The main motivation for refitting was to take advantage of the smaller uncertainties in the new version in some of the spectroscopic parameters used in fitting. Of the parameters used, S, n_{air}, and T change between the versions, and γ_{air} remains the same. However, the change in T is negligible. The most significant change between versions comes from the 1.24% increase in S, which in principle should cause a 1.24% decrease in retrieved concentrations. The -5.48% change in n_{air} results in a small change in retrieved concentrations at the low pressures and temperatures found in the IsoCloud experiments. The uncertainty in S changes significantly between versions, from 5% in the 2012 version to 1% in the 2016 version. The parameters for the H_2O transition at 3789.6348 cm^{-1}, their uncertainties, and the change between versions are shown in Table S2.

Param	2012	2016	Δ (%)
S	$5.406 \times 10^{-22} \pm 5\%$	$5.473 \times 10^{-22} \pm 1\%$	1.24%
γ_{air}	$0.908 \pm 1\%$	$0.908 \pm 1\%$	0%
n_{air}	$0.73 \pm 10\%$	$0.69 \pm 10\%$	-5.48%
T	275.497	275.4971	0.00004%

Table S2. Spectroscopic parameters used to extract concentrations from the raw spectra, and their values in the 2012 and 2016 HITRAN databases. Where applicable, the associated uncertainties of each quantity are also presented as a percent. S has units of cm^{-1}/molecule cm^{-2}, γ_{air} has units of cm^{-1}, n_{air} is a dimensionless quantity, and T has units of K. The final column represents the percent change of the 2016 value with respect to the 2012 value.

In practice, refitting with the new HITRAN 2016 parameters yields concentrations that are slightly more than 1% less than those fit with the HITRAN 2012 parameters. This change in concentration does not change the conclusions drawn from the analysis presented in the main text, although it does result in a somewhat lower estimate of the saturation vapor pressure of ice I_h for the ATD values.

In addition to the new spectroscopic parameters, the data were refit using an updated version of ICOSfit. Comparison fits between the two versions were done by fitting the same spectra with the same spectroscopic parameters and comparing the results. These tests show no significant difference in retrieved concentrations that can be attributed to the version of ICOSfit used.

For completeness, we present here the original results of the analysis which used concentrations retrieved using the 2012 HITRAN parameters. It is important to note that we also improved our calculation of uncertainties at the same time as we refit the data, which in general led to larger error bars. Thus the error between the two versions looks roughly the same, despite the fact that the uncertainty on S decreased significantly. Note that in the HITRAN 2012 version of the figure, the vapor pressure estimate given in Shilling et al. (2006) has no temperature dependence, but in the HITRAN 2016 version of the figure we have included and estimate of its temperature dependence.

S5 Tables of Experiments

References

Gordon, I. E., Rothman, L. S., Hill, C., Kochanov, R. V., Tan, Y., Bernath, P. F., Birk, M., Boudon, V., Campargue, A., Chance, K. V., and et al.: The HITRAN2016 Molecular Spectroscopic Database, Journal of Quantitative Spectroscopy and Radiative Transfer, doi:10.1016/J.JQSRT.2017.06.038, 2017.

Korolev, A. V. and Mazin, I. P.: Supersaturation of Water Vapor in Clouds, Journal of the Atmospheric Sciences, 60, 2957–2974, doi:10.1175/1520-0469(2003)060<2957:SOWVIC>2.0.CO;2, https://doi.org/10.1175/1520-0469(2003)060<2957:SOWVIC>2.0.CO;2, 2003.

Rothman, L., Gordon, I., Babikov, Y., Barbe, A., Benner, D. C., Bernath, P., Birk, M., Bizzocchi, L., Boudon, V., Brown, L., Campargue, A., Chance, K., Cohen, E., Coudert, L., Devi, V., Drouin, B., Fayt, A., Flaud, J.-M., Gamache, R., Harrison, J., Hartmann, J.-M., Hill, C., Hodges, J., Jacquemart, D., Jolly, A., Lamouroux, J., Roy, R. L., Li, G., Long, D., Lyulin, O., Mackie, C., Massie, S., Mikhailenko, S., Müller, H., Naumenko, O., Nikitin, A., Orphal, J., Perevalov, V., Perrin, A., Polovtseva, E., Richard, C., Smith, M., Starikova, E., Sung, K., Tashkun, S., Tennyson, J., Toon, G., Tyuterev, V., and Wagner, G.: The HITRAN2012 molecular spectroscopic database, Journal of Quantitative Spectroscopy and Radiative Transfer, 130, 4 – 50, doi:https://doi.org/10.1016/j.jqsrt.2013.07.002, hITRAN2012 special issue, 2013.

Shilling, J. E., Tolbert, M. A., Toon, O. B., Jensen, E. J., Murray, B. J., and Bertram, A. K.: Measurements of the vapor pressure of cubic ice and their implications for atmospheric ice clouds, Geophysical Research Letters, 33, L17 801, doi:10.1029/2006GL026671, 2006.

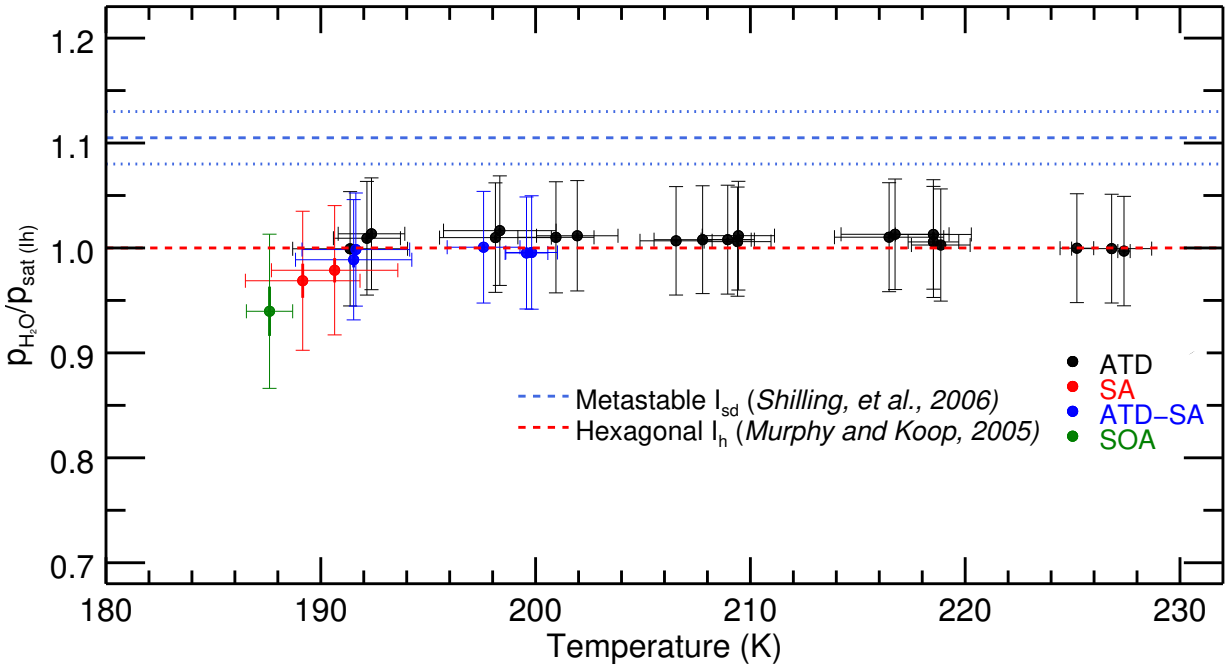

Figure S10. Results of the analysis using concentrations retrieved using the 2012 HITRAN parameters. Note that the error bars in this analysis are nearly the same size as those in the current analysis presented in the main paper, which is due to the fact that we also updated our uncertainty calculations between versions, which mainly served to increase the size of the error bars. Also note that Shilling's estimate of vapor pressure has no temperature dependence in this version.

Number	Aerosol/IN	T_0	ΔT	P_0	ΔP	$\frac{dn}{dt}/n$	$M_{i,max}$	r_{max}	τ	t_{exp}/τ	N_{max}	S_{max}	offset
3	ATD	233.4	-6.4	300	-100	-0.065%	26.1%	6.3	28	18.4	38	1.05	1.1
4	ATD	233.4	-9.1	300	-130	-0.091%	27.8%	6.2	22	32.2	44	1.09	2.1
5	ATD	233.5	-9.1	300	-100	-0.097%	34.7%	6.0	21	23.6	50	1.09	1.8
7	ATD	223.18	-6.4	234	-64	-0.063%	47.2%	3.7	22	21.3	90	1.03	0.43
8	ATD	223.3	-8.8	300	-130	-0.095%	60.0%	4.8	22	26	90	1.03	0.31
9	ATD	223.3	-6.0	300	-70	-0.062%	41.8%	3.9	26	14.8	65	1.03	0.24
10	ATD	223.1	-5.6	230	-60	-0.063%	39.4%	3.9	27	15.4	70	1.05	0.78
11	ATD	223.3	-8.9	300	-150	-0.096%	61.6%	4.1	20	26.3	94	1.09	0.36
13	ATD	213.1	-5.3	235	-65	-0.060%	44.9%	1.7	18	29.6	350	1.06	0.21
14	ATD	213.3	-8.4	300	-130	-0.079%	68.0%	1.7	12	56.9	480	1.07	0.16
15	ATD	213.3	-5.6	300	-170	-0.060%	40.6%	1.5	15	27.6	400	1.06	0.01
16	ATD	213.2	-5.4	234	-64	-0.061%	36.8%	1.5	16	30.0	450	1.04	0.12
17	ATD	213.3	-8.4	300	-130	-0.090%	53.8%	1.7	11	51.1	600	1.07	0.02
20	ATD	193.7	-4.8	240	-70	-0.055%	93.7%	0.9	55	21.0	210	1.18	0.27
21	ATD	193.7	-7.6	300	-130	-0.082%	136%	0.9	40	42.1	300	1.24	0.14
22	ATD	193.6	-7.5	300	-130	-0.081%	123%	1.0	53	31.4	180	1.28	0.10
24	ATD	204.2	-5.4	300	-70	-0.057%	57.0%	1.3	32	18.7	219	1.14	0.15
25	ATD	203.7	-5.0	234	-64	-0.057%	49.9%	1.2	41	13.4	193	1.10	0.25
26	ATD	203.8	-8.0	300	-130	-0.087%	79.4%	1.2	24	31.8	352	1.10	0.11
27	ATD	203.8	-8.1	300	-130	-0.087%	76..5%	1.2	24	29.6	373	1.09	0.10
30	SA	194.0	-7.6	300	-130	-0.083%	93.0%	1.4	154	8.2	65	1.90	0.13
31	SA	194.0	-7.6	300	-130	-0.083%	82.9%	1.5	199	5.7	39	1.85	0.15
32	SA-ATD	194.0	-7.6	300	-130	-0.083%	101%	1.1	86	13.8	115	1.31	0.07
33	SA-ATD	194.1	-7.6	300	-130	-0.083%	127%	0.9	41	33.5	250	1.22	0.12
35	SOA	189.0	-7.3	300	-130	-0.080%	116%	1.2	189	17.1	50	2.00	0.22
46	SA-ATD	204.1	-5.5	300	-70	-0.057%	39.1%	1.2	42	9.8	170	1.11	0.19
47	SA-ATD	203.9	-5.2	234	-64	-0.056%	36.2%	1.2	45	9.2	170	1.08	0.24
48	SA-ATD	203.9	-7.6	300	-130	-0.082%	52.3%	1.2	27	22.2	280	1.18	0.10

Table S3. Table of experiment included in the analysis. T_0 is the base temperature of the experiment before expansion begins, and ΔT gives the decrease in temperature from the start of the experiment to its coldest point. P_0 is the pressure in hPa before expansion begins, and ΔP is the decrease in pressure over the experiment. $\frac{dn}{dt}/n$ is the pumping rate expressed as the percentage of chamber molecules lost per second. This can also be thought of as the percentage of the chamber's volume that is evacuated each second. $M_{i,max}$ is the maximum ice mass in the chamber as a percentage of the vapor mass at the start of pumping. r_{max} is the maximum average ice particle radius. τ is the typical relaxation time in seconds during the portion of the experiment used in the analysis. N_{max} is the maximum ice particle number in cm^{-3}. S_{max} is the maximum saturation observed, typically when nucleation begins. Offset the difference between the scaled APeT measurement and ChiWIS which is subtracted from the rest of the experiment.

Number	Reason	T_0	Aerosol	N_{max}	τ	t_{exp}/τ
1	Short Pump	234	ATD	19	40	4.5
2	High τ	234	ATD	7	112	2.3
6	High τ	234	ATD	11	110	3.4
12	Ref	213	Ref	7	–	–
18	No ChiWIS	213	Ref	–	–	–
19	Ref	194	Ref	4	–	–
23	No ChiWIS	194	ATD	–	–	–
28	Ref	194	Ref	17	418	1.0
29	High τ	194	SA	14	419	0.6
34	Ref	189	Ref	13	553	2.2
36	High τ	189	SOA-HNO_3	3	248	2.1
37	No Welas 1	189	SOA-HNO_3	–	–	–
38	No Welas 1	189	SOA-HNO_3	–	–	–
39	Ref	223	Ref	1	–	–
40	Dry Wall	223	ATD	9	151	1.0
41	Dry Wall	223	ATD	15	86	5.4
42	Dry Wall	223	ATD	16	85	5.4
43	Dry Wall	223	ATD	17	68.2	7.4
44	Ref	204	Ref	23	197	1.7
45	High τ	204	SA	17	205	3.1

Table S4. Table of experiments excluded from analysis. T_0 is the temperature before expansion begins. Aerosol is the type of aerosol or ice nucleus the chamber has been prepared with. N_{max} is the maximum ice particle concentration observed in the chamber. τ is the relaxation time in seconds calculated at the time when N_{max} occurs.